J Mater Sci (2007) 42:4149–4158
DOI 10.1007/s10853-006-0893-y

Reaction sintering of intermetallic-reinforced composite materials

I. A. MacAskill · D. P. Bishop

Received: 17 January 2006 / Accepted: 28 August 2006 / Published online: 7 March 2007

Abstract The goal of this research was to explore the powder metallurgy (P/M) processing response of materials based on the Al–Ni system. In doing so, compacts of pure aluminum powder as well as binary Al–Ni blends were prepared, compacted, sintered, and assessed. Research began with fundamental studies on the sintering response of the base aluminum powder. This system demonstrated a poor sintering response overall but did improve at higher temperatures commensurate with a small fraction of a secondary phase that was presumed to be aluminum nitride. In Al–Ni systems sintering temperature had a particularly pronounced effect on the resultant microstructure. At lower temperatures a composite of Al–$NiAl_3$–AlN was formed while higher temperatures yielded one of Al–$NiAl_3$ alone. It was postulated that the exothermicity of $NiAl_3$ formation and the extent of matrix sintering were controlling factors for this behaviour.

Introduction

Powder metallurgy (P/M) is an advanced metal forming technique used to fabricate precision products in a near-net-shape manner. Fundamental stages of this process include powder blending, compaction, and sintering. The latter is often regarded as the most critical and as such, there are many different ways in which this step can be accomplished. One common approach involves compacts of dissimilar powders (typically elemental) that are sintered at an elevated temperature. In doing so, thermodynamic and kinetic driving forces engage so as to cause the powder species to react and eventually form a homogenous product comprised of new metallurgical phases in accordance with equilibrium predictions. A sintering strategy such as this is routinely used in the manufacture of products from conventional P/M iron [1], copper [2], and aluminum alloys [3] wherein alloying additions of an elemental nature (copper, nickel, tin, etc.) are blended together with the base powder itself. The associate reactions that occur during sintering are generally endothermic and occur at what amounts to a kinetically slow pace; the gradual manner of reaction helping to ensure accurate shape retention in the sintered product.

The same type of approach also finds frequent usage in the synthesis of more exotic materials such as high temperature, low density aluminides based on the Al–Ni [4], Al–Ti [5], and Al–Fe [6] systems to name but a few. The starting raw powders are again elemental in nature and are initially blended in the required stoichiometric ratio so as to facilitate complete reaction into the intended product—a single phase intermetallic rich in the transition metal. However, unlike the aforementioned conventional materials, these processes are highly exothermic ensuring that a considerable amount of heat is liberated. As such, this type of practice is more commonly referred to as ''reaction sintering''. While this can be a viable means to synthesize intermetallics, distortion and a high level of porosity that result from the excessive heat flow are

I. A. MacAskill · D. P. Bishop (✉)
Department of Process Engineering and Applied Science, Dalhousie University, 1360 Barrington St., Halifax, B3J 2X4 Nova Scotia, Canada
e-mail: Paul.Bishop@Dal.ca

known areas of concern [7, 8]. In an attempt to capitalize on the mechanical properties of intermetallics yet reduce exothermic heat flow and thereby retain the near-net-shape benefits of conventional P/M, the authors have investigated reaction sintering of aluminum-rich Al–Ni binary mixtures. The intent being to form a near-net-shape composite material comprised of an aluminum matrix reinforced by an intermetallic(s) using conventional ''press and sinter'' P/M technology.

Experimental techniques

The P/M processing route followed included stages of powder blending, uni-axial die compaction and sintering. With regards to the former, all powders (including the addition of 1.5% wax lubricant) were initially weighed to an accuracy of 0.01 g and then blended in a Turbula mixer for 20 min. To compact powder blends an Instron 5594–200 HVL load frame (1,000 kN capacity) was used in conjunction with self-contained tooling that incorporated a floating-die concept. Using this system powders were briquetted at 400 MPa into transverse rupture strength (TRS) bars (~9 mm × 12.7 mm × 31.8 mm).

Groups of intact TRS bars were then sintered in nitrogen in a controlled atmosphere tube furnace. Sintering temperatures ranged form 520 °C to 640 °C. The details of the sintering process are given elsewhere [9]. The techniques used to asses an alloy's response to sintering included the measurement of green and sintered densities, dimensional change, and apparent hardness in the Rockwell ''H'' scale. Thermal analyses were then completed for select combinations of alloy/sintering temperatures using a Netzsch 402C thermal dilatometer and a Netzsch STA 409 PG/PC combined DSC/TGA. All samples for such tests were initially dry cut from green TRS bars and de-lubricated under flowing nitrogen in a separate furnace so as to avoid instrument contamination. Preliminary calibration of the dilatometer was performed with a sapphire standard using an applied load of 30 cN. A dynamic nitrogen flow rate of 50 ml/min was maintained in both instruments during the tests following a preliminary purge/evacuation sequence.

To assess microstructural features cross-sections of sintered TRS bars were subjected to conventional metallographic preparation techniques. The microstructure was then characterized via Electron-Probe Micro-Analysis (EPMA). All such efforts were performed on carbon coated samples using a JEOL JXA-8200 WD/ED combined micro-analyzer operating in wavelength dispersive mode at an accelerating voltage of 15 kV. At the beginning of each session the instrument was calibrated using a set of elemental and compound standards. The reported chemistry of each phase represents an average of ten point scan analyses. The final aspect of microstructural characterization was X-ray diffraction (XRD) wherein specimens were examined under filtered Cu Kα radiation using a Rigaku^{TM} XRD unit. Operating parameters included an applied voltage of 40 kV, tube current of 40 mA, and a 2θ scan speed of 4 deg/min over the range of 10 to 100°.

Materials

Air atomized aluminum powder (D_{50} of 107 μm) from Ecka-Granules was the basis of all blends. INCO Grade 123 was selected as the source of nickel. This powder was supplied by GKN Sinter Metals and had a D_{50} of 10 μm as measured by laser particle size analysis. SEM micrographs of these powders are shown in Fig. 1. Prior to use the chemistries of each were analyzed using wet chemical analysis coupled with atomic adsorption to confirm their compositions and to test for the presence of trace elements (Table 1).

Results and discussion

Sintering response of aluminum powder

To study the sintering response of the base aluminum powder compacts were prepared and sintered at a variety of temperatures. Data on dimensional change as a function of sintering temperature is presented in Fig. 2. Compacts of the base aluminum powder experienced minimal dimensional change until a sintering temperature of 630 °C was employed. At this temperature a transition from expansion to shrinkage was observed. Commensurate with this transition were an increase in sintered density and a decrease in interconnected porosity (Fig. 3). Apparent hardness data was consistent with these observations as samples sintered at the lower temperatures were too soft to be measured while a modest improvement to 20 HRH occurred at 630 °C.

To further investigate the effect of sintering temperature additional green samples were heated in a thermal dilatometer under conditions below (580 °C) and at (630 °C) the onset of shrinkage. Results of these runs are shown in Fig. 4. Both compacts experienced an identical response up to the respective sintering temperatures. When held at 580 °C no dimensional change was observed such that upon cooling back to

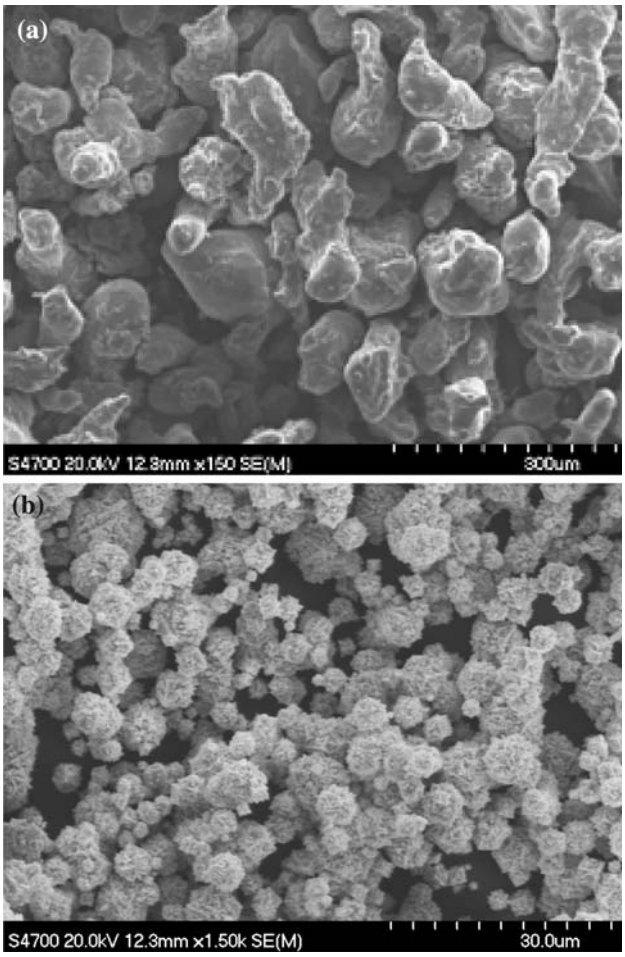

Fig. 1 SEM images of raw powders. (**a**) Air atomized aluminum and (**b**) carbonyl nickel

ambient the net dimensional change was effectively zero and the original dimensions were restored. Conversely, an isothermal hold at the higher temperature resulted in progressively increasing shrinkage throughout the dwell period, indicating that sintering had progressed to some extent. The net change for this specimen was approximately 0.2% shrinkage. These observations were consistent with measurements of sintered TRS bars as shown in Fig. 2.

To assess the microstructure and sinter quality EPMA and XRD analyses were completed. Compositional mode images of the base aluminum powder sintered at the same two temperatures employed in the aforementioned dilatometer studies are shown in

Table 1 Chemical assays of metal powders (w/o)

Powder	Al	Mg	Ni	Si	Cu	Fe	Zn	Mn	C	S
Al	99.9	0.01	0.03	0.10	0	0.08	0	0.001	–	–
Ni	–	–	99.3	–	–	0.11	–	–	0.13	0.002

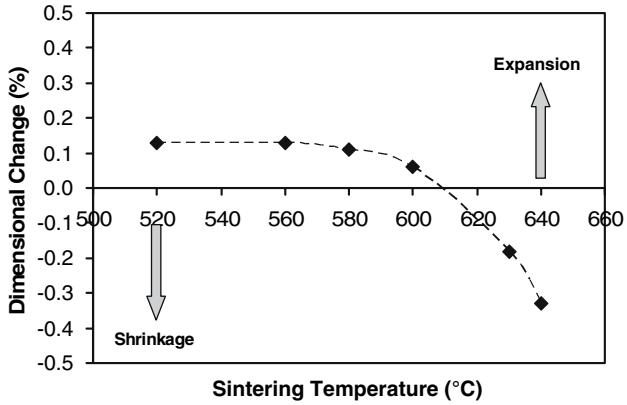

Fig. 2 Dimensional change as a function of sintering temperature for aluminum powder compacts

Fig. 5. The sinter quality was clearly poor in both instances given the abundance of prior particle boundaries along with a lack of appreciable interparticle necking, pore rounding, and grain growth. WDS analyses (Table 2) implied the sole presence of α-aluminum. Interestingly, this feature contained a consistently measurable amount of nitrogen in specimens held at the higher temperature.

Subsequent work via XRD implied the exclusive presence of α-aluminum at all sintering temperatures. Since XRD failed to identify any nitrogen-bearing phases, bars of the base aluminum sintered at 580 and 630 °C were fractured and the internal structure examined. The fracture surface from the specimen sintered at the lower temperature was essentially featureless except for an abundance of prior particle boundaries (Fig. 6a). At the higher temperature a secondary phase was noted within the pores (Fig. 6b). Examination at increased magnification indicated that this phase had a spiky topography and a nodular character. EDS analyses

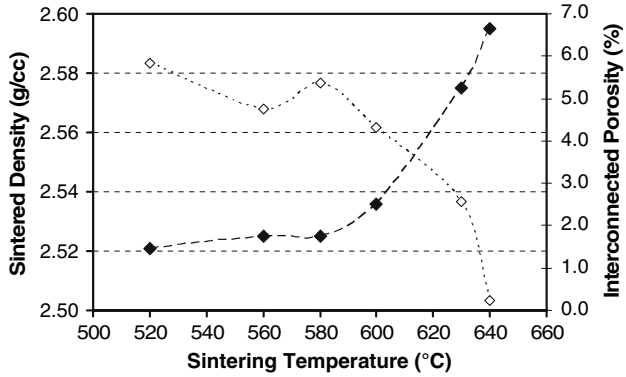

Fig. 3 Sintered density and interconnected porosity as functions of sintering temperature for air atomized aluminum

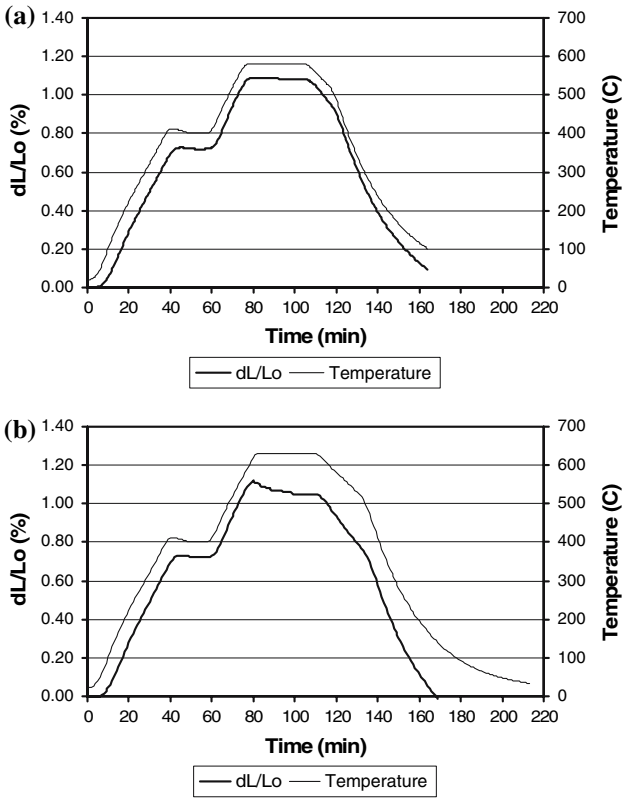

Fig. 4 Thermal dilatometry curves for compacts made from air atomized aluminum powder sintered at (**a**) 580 °C and (**b**) 630 °C

confirmed nitrogen enrichment but the small size prevented accurate, quantitative assessment.

Sintering response of Al–Ni compacts

Binary Al–Ni compacts were then fabricated and sintered. As noted earlier, the pure base powder of aluminum did not exhibit any shrinkage until compacts were sintered at temperatures of 630 °C or higher. Furthermore, the onset of shrinkage correlated well with increases in density and apparent hardness in the same temperature regime. The addition of nickel altered this sintering response significantly.

Notably, all of the Al–Ni alloys experienced appreciable swelling (Fig. 7) when sintered in the range of 520 °C to 600 °C. This effect scaled directly with nickel content reaching a maximum near 4% expansion for Al–15Ni specimens. As with the base aluminum, densification was eventually observed at higher sintering temperatures. Measurements of sintered density were supportive of these results as a reduced density was noted for samples sintered at low temperatures wherein swelling occurred while an appreciable increase was observed at higher temperatures once shrinkage had become operative (Fig. 8). Increases in sintering temperature also resulted in decreased interconnected porosity (IP) (Fig. 9). Intuitively, it was expected that the swelling and low density that were synonymous with lower sintering temperatures would yield poor apparent hardness. Experimental results (Fig. 10) contradicted this notion and revealed that the highest hardness values actually occurred at lower sintering temperatures. Furthermore, the attenuation of maximum hardness was displaced to progressively lower sintering temperatures as the nickel content was increased (i.e. 600 °C with 6 w/o nickel down to 580 °C with 15 w/o).

To establish the reasoning for this behaviour, thermal analyses were completed at the two transition temperatures—580 °C (maximum hardness and swelling) and 630 °C (reduced hardness but demonstrable shrinkage). Dilatometry results (Fig. 11) were in stark contrast to each other and to previous data for the base aluminum powder itself (Fig. 4). Here, both samples exhibited significant swelling as they were heated to their respective sintering temperatures. However, the swelling was quickly reversed in the sample sintered at 630 °C such that the final dimensional change for the cooled specimen was actually a net shrinkage of ~0.6%.

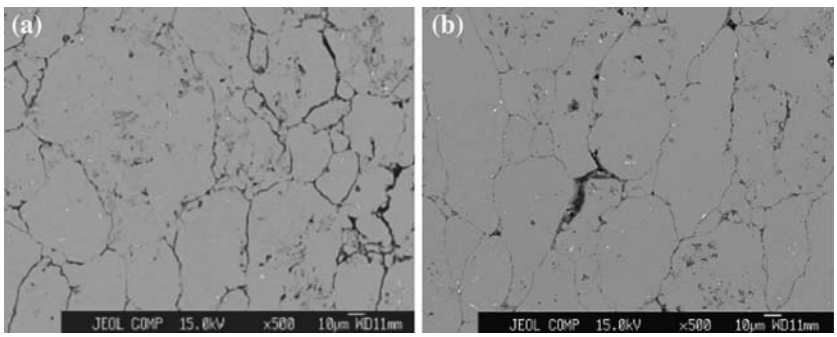

Fig. 5 Compositional mode SEM images of aluminum powder compacts sintered at (**a**) 580 °C and (**b**) 630 °C

Table 2 Averaged and normalized compositions of the principal phases noted in the compacts prepared from pure Al powder shown in Fig. 5

Point #	Sintering Temperature	Region	Chemistry (w/o)				
			Al	Ni	Mg	N	Fe
1	580 °C	α-Aluminum	Bal.	0.00	0.00	0.00	0.05
1	630 °C	α-Aluminum	Bal.	0.01	0.00	0.64	0.01

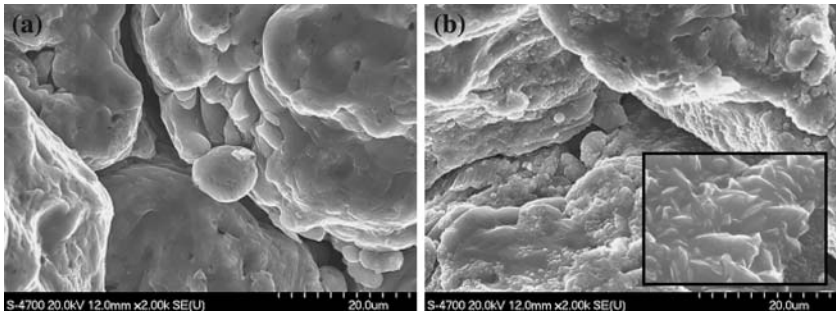

Fig. 6 Comparison of the internal structures noted in samples of the base aluminum powder sintered at (**a**) 580 °C and (**b**) 630 °C. A spiky, nodular feature (see inset of (**b**)) was present in the pores of the specimen sintered at the higher temperature

At 580 °C this reversal was effectively absent as the finished sample retained its swollen state even after cooling to ambient wherein a resultant dimensional change of ~3.5% expansion ensued.

DSC/TGA analyses of the Al–15Ni compacts at the same temperatures of interest are presented in Fig. 12. DSC data on the base aluminum powder revealed that no identifiable peaks were present regardless of sintering temperature and that a static heat flow was maintained for the entirety of the isothermal hold at the sintering temperature. Comparatively, DSC traces of the Al–15Ni samples showed evidence of obvious exothermic behaviour. In this regard, a gradual exothermic response engaged at approximately 520 °C in both samples. Increased exothermicity persisted in that sintered at 580 °C until the isothermal hold was initiated. Once held at this temperature the heat flow initially reversed but then again resumed a gradually increasing exothermic response during the 30 min period. For the sample sintered at 630 °C, continued heating beyond 580 °C brought about a sharp exothermic peak much deeper than that observed at the lower sintering temperature. The exothermic response then ended as soon as the isothermal hold engaged after which time a static heat flow akin to that of the base aluminum itself ensued. Corresponding TGA data

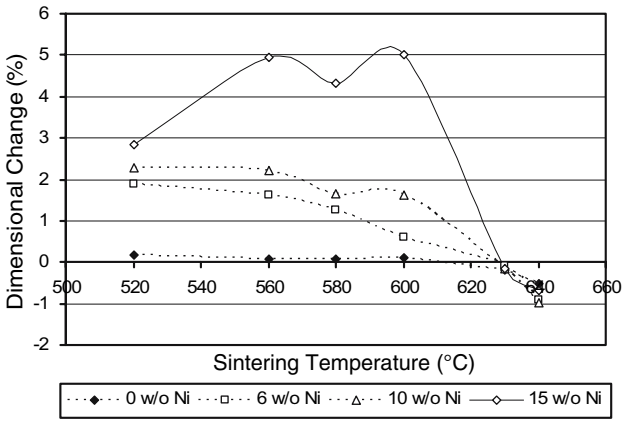

Fig. 7 Dimensional change as a function of sintering temperature for Al–XNi compacts

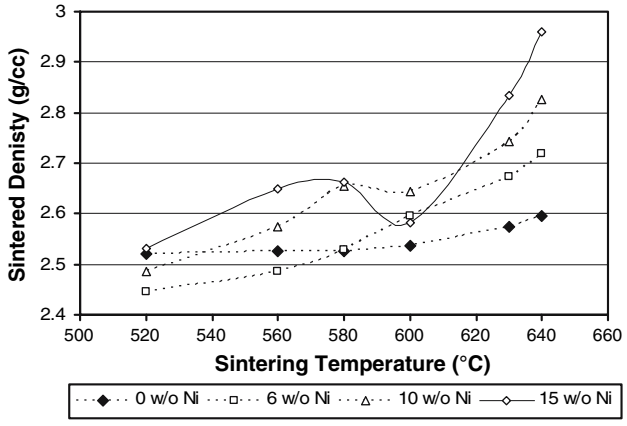

Fig. 8 Sintered density as a function of sintering temperature for Al–XNi alloys

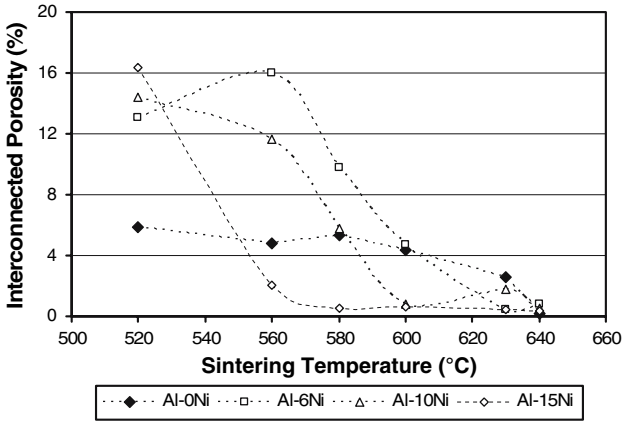

Fig. 9 Interconnected porosity as a function of sintering temperature for Al–XNi alloys. The sharp drop in IP shifts to lower temperatures as the nickel content is increased

indicated that all samples experienced some level of weight gain during the isothermal hold. For the base aluminum and the Al–15Ni sintered at 630 °C the gains were minimal; ~0.25 w/o and 0.5 w/o respectively. Interestingly, a considerably greater gain was noted for Al–15Ni sintered at 580 °C (~1.5 w/o).

Microstructural analyses were then completed on the Al–Ni specimens. Considering Al–15Ni alloys, the microstructures of such samples were in stark contrast (Fig. 13). At the lower temperature the structure was comprised of a bright phase encased in an apparent reaction zone and dispersed within a dark grey matrix. WDS analyses (Table 3) indicated that the matrix was α-aluminum containing ~1 w/o nitrogen. The bright phase had a nominal composition that correlated well with the intermetallic $NiAl_3$ (42 w/o Ni + 58 w/o Al); this was consistent for all nickel contents investigated.

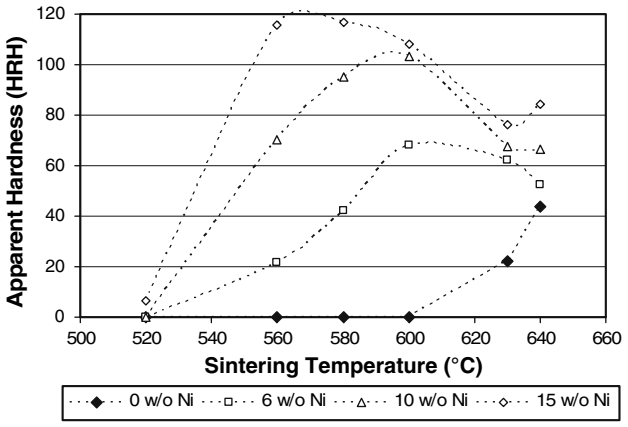

Fig. 10 Apparent hardness as a function of sintering temperature for compacts made from various Al–XNi (X = 0, 6, 10, 15 w/o) binary formulations

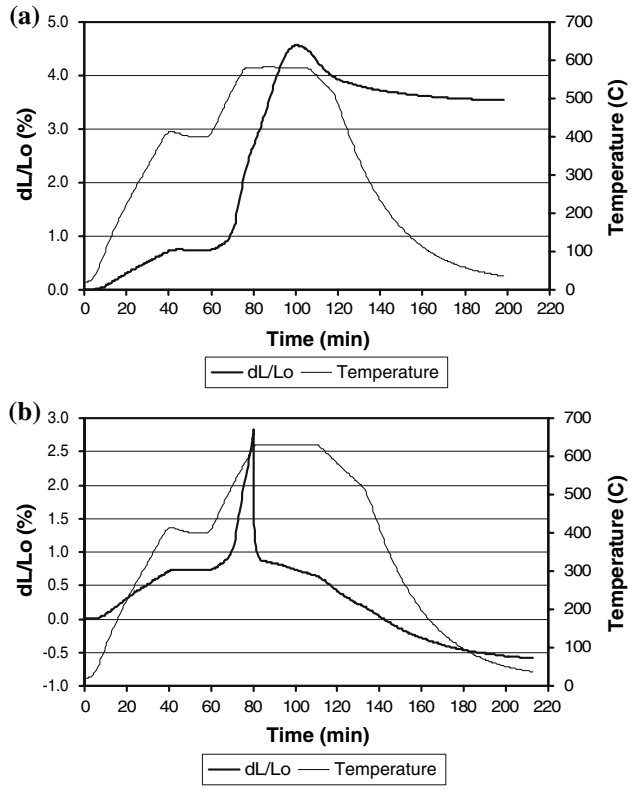

Fig. 11 Thermal dilatometry curves for Al-15Ni compacts sintered at (**a**) 580 °C and (**b**) 630 °C

Analyses of the reaction zone revealed a pronounced enrichment of nitrogen of ~11 w/o (Table 3). Subsequent XRD work indicated that the principal phases were α-aluminum, $NiAl_3$, and AlN (Fig. 14). Since WDS analyses were not compliant with that of pure AlN (34.2 w/o N) this suggested that the reaction zone was a multi-phase region most likely comprised of α-aluminum plus AlN.

When sintered at the higher temperature (630 °C) the presence of α-aluminum and $NiAl_3$ was again confirmed (Figs. 13 and 14; Table 3). However, there was a notable absence of the reaction zone. The latter was consistent with an absence of AlN peaks in XRD spectra. Additional XRD tests on Al–15Ni samples sintered in the range of 520–630 °C indicated that all alloys contained $NiAl_3$ and that only those sintered at the lowest temperature contained the precursory Ni_2Al_3. No samples were found to contain any elemental nickel or any other binary intermetallics. As evident by variations in the intensity of the principal peak for AlN, this phase was only present when intermediate sintering temperatures (560 to 600 °C) were employed (Fig. 15).

As with samples of the base aluminum, compacts made from the Al–15Ni sintered at low (580 °C) and

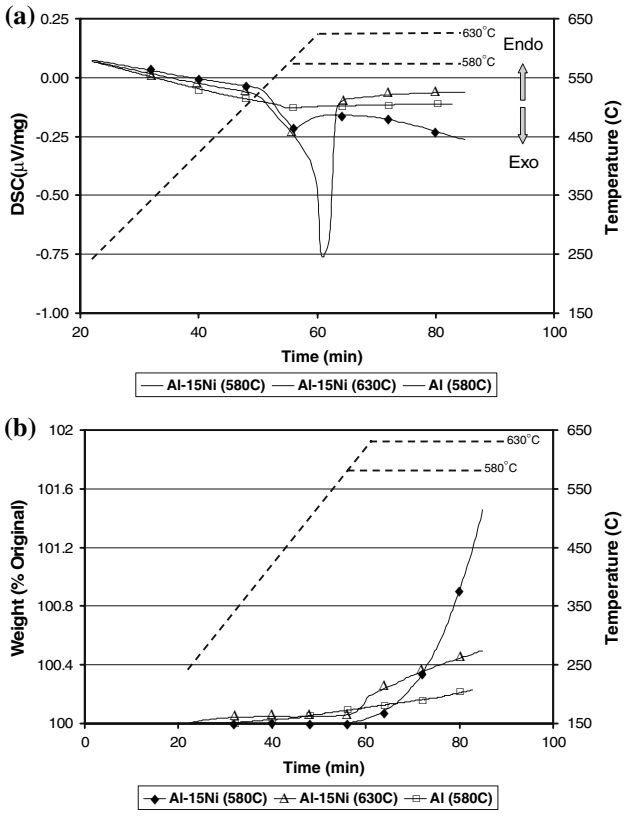

Fig. 12 Thermal analyses of pure aluminum and Al–15Ni compacts sintered at 580 °C and 630 °C. (**a**) DSC analyses and (**b**) corresponding weight change data

high (630 °C) temperatures were fractured and examined in the SEM (Fig. 16). At the lower temperature the surface was principally comprised of flat facets coupled with a spiky phase that completely lined the pores. EDS analyses confirmed that the former corresponded to fracture through $NiAl_3$ particles while the latter feature was nitrogen enriched. At the higher temperature the facets persisted yet no nitrogen-bearing phases were detected.

Discussion

The intent of this research was to initiate the development of aluminum P/M materials based on the Al–Ni system. Work began with a fundamental study of the base aluminum itself. Compacts of pure aluminum powder exhibited a poor sintering response and failed to develop any appreciable mechanical integrity. While this came as no surprise to the authors, signs of improvement were noted at the highest sintering temperatures considered. For example, sintering at 630 °C resulted in measurable shrinkage and concomitant increases in sintered density and apparent hardness.

Commensurate with such improvements was the presence of a measurable quantity of nitrogen within the α-aluminum constituent (Table 2). XRD techniques failed to identify any nitrogen-bearing phases in this sample, but SEM examination confirmed that a nitrogen-enriched feature existed within the pores. Interestingly, the general nature of this phase was quite similar to work by Kondoh et al [10] wherein the in-situ formation of aluminum nitride (AlN) in aluminum P/M alloys was studied. In their work the authors sintered prealloyed Al–12Si–2Ni–1Mg power at 550 °C in nitrogen for prolonged periods (5 h). Under these conditions they were eventually able to grow the nodular feature to the point where it was detectable via XRD. This phase was then identified as AlN. Given the morphological similarities and confirmed nitrogen enrichment, it is postulated that the film/nodular feature noted in this work was also AlN. In this way, the higher temperature has yielded a reaction between aluminum and the surrounding atmosphere as has been observed by others for pure aluminum powder [11].

Having established the sintering response of the base aluminum and that a reaction between it and the surrounding gaseous atmosphere was likely, research was then directed at the effects of nickel. Aluminum and nickel powders should react and

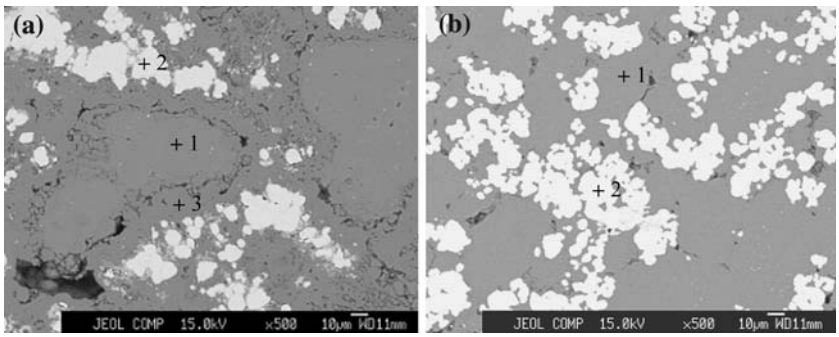

Fig. 13 Compositional mode SEM images of Al-15Ni sintered at (**a**) 580 °C and (**b**) 630 °C

Table 3 Averaged and normalized compositions of the principal phases noted in the experimental alloy Al–15Ni shown in Fig. 13

Point #	Sintering Temperature	Region	Chemistry (w/o)				
			Al	Ni	Mg	N	Fe
1	580 °C	α-Aluminum	Bal.	0.30	0.01	0.98	0.01
2		$NiAl_3$	Bal.	40.08	0.00	0.21	0.10
3		Reaction Zone	Bal.	0.81	0.00	10.95	0.00
1	630 °C	α-Aluminum	Bal.	0.47	0.00	0.00	0.00
2		$NiAl_3$	Bal.	40.67	0.00	0.00	0.14

eventually form α-aluminum and $NiAl_3$ in accordance with binary phase diagram predictions for the compositions investigated. This was confirmed via XRD as both phases were detected at all temperatures. Aluminum nitride was also present but only under select processing conditions (Figs. 14, 15). Here, appreciable concentrations of this phase were readily noted at intermediate (~580 °C) temperatures yet it was effectively absent at the higher (630 °C) and lower (520 °C) extremes. It is postulated that this response was the result of observed variations in the exothermicity of $NiAl_3$ formation coupled with AlN nucleation throughout the compact. Consider first the condition that led to maximum nitridation (580 °C sintering temperature). In this situation the reaction to form $NiAl_3$ was confirmed to be complete, yielding significant swelling of the compact (Fig. 11). In addition, it was also found to be moderately exothermic (Fig. 12). The associate heat would have temporarily raised the temperature of the compact so as to initiate a secondary reaction between the base aluminum and nitrogen atmosphere to form AlN; also known to be exothermic [12, 13]. In a swollen state, channels of IP would have remained open to the surrounding atmosphere allowing the ingression of a continuous supply of fresh nitrogen so as to sustain the nitridation response. The exothermic character as well as reaction sustenance were both confirmed via DSC/TGA given that a gradually increasing exothermic response as well as a continual weight gain were observed throughout the entire isothermal hold at 580 °C (Fig. 12). Once formed, AlN effectively locked in the swollen configuration and minimized contraction due to subsequent sintering or thermal relaxation upon cooling (Fig. 11). The reaction was ultimately self-starving as AlN grew, thereby reducing the IP of the compact and in turn, the provision of one reactant species (gaseous nitrogen).

At 630 °C the situation was somewhat different. Here, DSC confirmed that the formation of $NiAl_3$ was far more exothermic in nature. This would have heated the compact up to the point where AlN could be nucleated but also enabled appreciable sintering of the

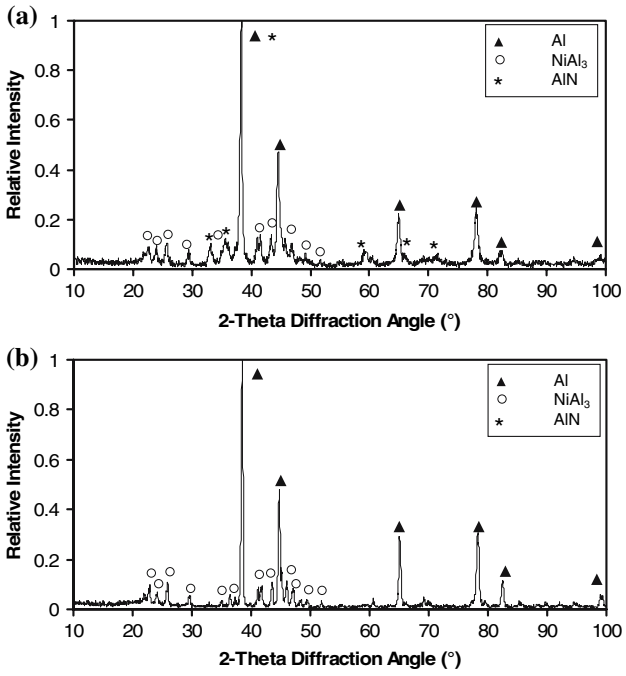

Fig. 14 XRD spectra for Al-15Ni binary alloys sintered at (**a**) 580 °C and (**b**) 630 °C

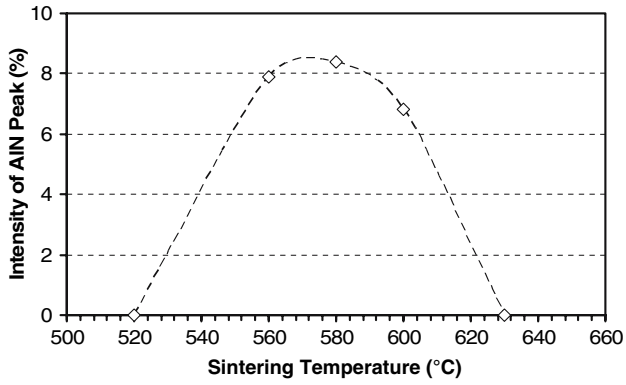

Fig. 15 Change in intensity of the principal peak for AlN (d = 2.70Å) as a function of sintering temperature for Al–15Ni compacts

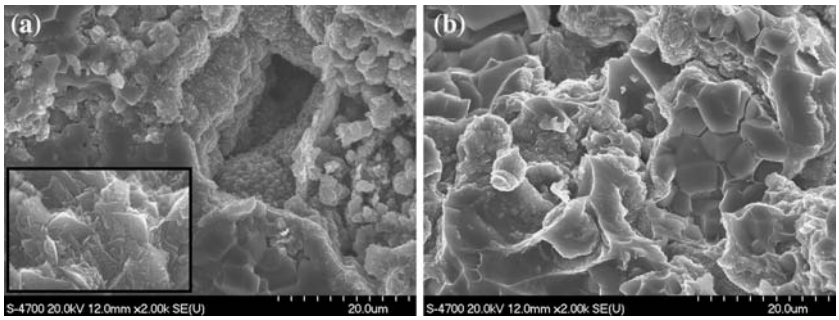

Fig. 16 Comparison of the internal structures noted in Al–15Ni samples sintered at (**a**) 580 °C and (**b**) 630 °C

aluminum matrix itself. The latter would have depleted the presence of IP and the inward flow of nitrogen so as to starve the nitridation process. The dimensions of the compact were then able to relax after aluminide formation allowing densification to proceed during sintering as expected (Fig. 11). A static heat flow during the isothermal hold (Fig. 12) implied that no further reactions occurred which was also supportive of a lack of obvious nitridation. Although a minor weight gain was realized, this was presumably a result of minimized nitride nucleation coupled with oxidation due to the presence of trace levels of gaseous oxygen in the DSC atmosphere.

Significant quantities of AlN had a decidedly positive effect on apparent hardness. Heavily nitrided samples attained hardnesses in excess of 110HRH under select processing conditions. This surpasses that of commercial press and sinter aluminum P/M alloys in the T1 condition. For example, A6061-T1 has a hardness of 80–85 HRH while that of AC2014-T1 is 55–60 HRE (~90 HRH) [14]. Given that apparent hardness (Fig. 10) tracked well with AlN concentration (Fig. 15) it is clear that this phase was responsible for the high hardness observed.

Conclusions

From the work completed the following conclusions have been reached:

1. The sintering response of pure aluminum powder was poor in a nitrogen atmosphere. Minor improvements were noted with elevated sintering temperature. It appeared that the formation of small nodules of AlN was associated with an improved sinter quality.
2. EPMA/XRD confirmed that all elemental nickel additions reacted with aluminum to form $NiAl_3$.
3. Sintering temperature had a particularly pronounced effect on the resultant microstructure of Al–Ni alloys; at lower temperatures a composite of Al–$NiAl_3$–AlN was formed while higher temperatures yielded one of Al–$NiAl_3$ alone.
4. It was observed that AlN only formed under select sintering conditions. It was deduced that its formation required a fresh supply of N_2 gas and an energy source supplied from the exothermic formation of $NiAl_3$.
5. Certain alloys exhibited an apparent hardness in excess of 110 HRH which was attributed to a considerable fraction of AlN within the microstructure

Acknowledgements The authors would like to acknowledge financial support from the Natural Sciences and Engineering Research Council of Canada (NSERC) and Mr. Ian Donaldson, Director of Research and Development, GKN Sinter Metals (Romulus, Michigan, USA). Hans-Claus Neubing (Eckart Granules, Fuerth, Germany) is gratefully acknowledged for his contribution of powders as are Drs. William Caley and Mahesh Chaturvedi (University of Manitoba, Canada) for their assistance with XRD.

References

1. Danninger H, Pottschacher R, Bradac S, Salak A, Seyrkammer J (2005) Powd Metall 48(1):23
2. Zadra M (2001) Int J Powd Metall 37(7):13
3. Bishop DP, Hofmann B, Couchman KR (2000) In: Ferguson H and Whychell DT (eds) Advances in Powder Metallurgy and Particulate Materials. MPIF, 1(12):87
4. Sims DM, Bose A, German RM (1988) Metal Powd Rep 43(9):563
5. Chiu LH, Nagle DC, Bonney LA (1999) Metall Mater Trans A 30A:781
6. Godlewska E, Szczepanik S, Mania R, Krawiarz J, Kozinski S (2003) Intermetallics 11:307
7. Wegmann MR, Misiolek WZ, German RM (1991) Advances in Powder Metallurgy, vol 2, Part 2. MPIF, p 175
8. Lee JH, Jung JC, Won CW (2002) J Mater Sci 37:2435

9. Hennessey CH, Caley WF, Kipouros GJ, Bishop DP (2005) Int J Powd Metall 41(1):50
10. Kondoh K, Kimura A, Watanabe R, (2001) Quart J Jap Weld Soc 19(2):383
11. Schaffer GB, Hall BJ, (2002) Metall Mater Trans A 33A:3279
12. Selvaduary S, Sheet L (1993) Inst Mater 463
13. Lee J, Lee I, Kim D, Ahn J, Chung H (2005) J Mater Res 20(3):659
14. ASTM International (2005) In: Annual Book of ASTM Standards 2005, Section Two – Nonferrous Metal Products. ASTM International, p 312